Transient Current Interruption Characteristics of a Novel Mechanical DC Circuit Breaker

Weijie Wen, Yizhen Wang, Bin Li, Yulong Huang, Ruisheng Li, and Qingping Wang

***Abstract*—With the rapid development of multiterminal direct current (MTDC) grids, high-voltage direct current circuit breakers (HV-DCCB) capable of interrupting currents within 5 ms are in urgent demand. The mechanical DCCB has always been one of the main proposals for HV-DCCBs. The current commutation is the prerequisite for mechanical DCCBs to interrupt currents successfully. Focused on the current commutation difficulty, a novel mechanical DCCB has been investigated in this paper. A simulation model of the novel mechanical DCCB in MTDC system for fault current interruption was established in PSCAD. By analyzing the simulation results, the detailed transient varying patterns of current, voltage, and energy in the novel mechanical DCCB during its interruption process are revealed. To verify the feasibility of the novel mechanical DCCB, a prototype was developed in the lab, and current interruption tests were carried out on the prototype. Experimental results have shown that a current of 5.3 kA can be interrupted by the prototype within 3 ms. In the end, failures that occurred in initial experiments are discussed and relative protection measures have been proposed. By adopting these measures, failures are successfully avoided and the normal operation of the novel mechanical DCCB are ensured.**

***Index Terms*—Current commutation, dc circuit breaker, failure mechanism, transient current interruption characteristics.**

I. Introduction

THE voltage source converter-based multiterminal direct current grid (VSC-MTDC) is widely recognized as a promising solution to integrate distant renewable energy sources, such as solar and wind energy, into ac networks [1]. To isolate short-circuit fault lines and improve the reliability of MTDC grids, high-voltage direct current circuit breakers (HV-DCCB) with the ability to interrupt direct fault current larger than 10 kA within 5 ms are in urgent demand [2]–[4]. Up to now, there are mainly two kinds of HV-DCCBs, which are hybrid DCCBs and mechanical DCCBs [5]–[7]. With advantages of the long research history, low operating losses, and low capital cost, the mechanical DCCB has drawn extensive attention and this paper is focused on key technologies relative to the mechanical DCCB.

Generally, the mechanical DCCB consists of three parallel paths, including a load current path, a commutation path, and an energy absorption path. In normal state, load current is conducted by the load current path composed of mechanical switches (MS), and operating losses of DCCB are so small that they can be neglected. Once a fault is detected, the current should be commutated from the load current path to the commutation path, whose key component is a high-voltage capacitor (C). After the current commutation, with the fault current charging C, the voltage across DCCB (UCB) increases continuously. As metal oxide varistors (MOVs) constitute the energy absorption path, when UCB increases to a certain value, the fault current is naturally commutated from the commutation path to the energy absorption path. After the current is commutated to the energy absorption path, UCB is limited to be the clamping voltage of MOVs and with the residual energy in MTDC grids being dissipated by MOVs, the fault current decreases gradually to zero. Thus, the current commutation from the load current path to the commutation path is the prerequisite for mechanical DCCBs to interrupt currents successfully.

By review of the previous studies, it is found that methods to produce current zero-crossing points by superimposing an oscillatory current on the direct arc current through MS have been employed to realize the current commutation in mechanical DCCBs. The current commutation methods can be divided into two kinds which are the self-excited oscillation method [8], [9] and the active-excited oscillation method [7], [10]–[14]. Topologies of mechanical DCCBs based on the two methods are illustrated in Fig. 1, respectively. As show in Fig. 1, the mechanical DCCB consists of three parallel paths and two disconnectors (K1 and K2) are installed at its both ends to interrupt the residual current.

The mechanical DCCB shown in Fig. 1(a) is based on self-excited oscillation. The self-excited oscillatory current (I_{hf}) in the closed circuit with the load current path and the commutation path in series is produced by the characteristic that SF6 arc voltage has downward gradient against a rising arc current [8], which means the arc extinguishing medium in MS of the load current path must be SF6. Limited by the amplitude of SF6 arc voltage, the maximum current that can be commutated and interrupted by this kind of mechanical DCCB is usually less than

Manuscript received October 13, 2017; revised December 14, 2017; accepted January 16, 2018. Date of publication January 24, 2018; date of current version August 7, 2018. This work was supported in part by the China Postdoctoral Science Foundation under Grant 2017M621071, in part by the National Natural Science Foundation of China under Grants 51677126 and 51677095, and in part by the National key R & D Plan (under Grant 2017YFB0902404). Recommended for publication by Associate Editor C. N. M. Ho. *(Corresponding author: Yizhen Wang.)*

W. Wen, Y. Wang, and Bin Li are with the Key Laboratory of Smart Grid of Ministry of Education, Tianjin University, Tianjin 300072, China (e-mail: weijie.wen@tju.edu.cn; yizhen.wang@tju.edu.cn; binli@tju.edu.cn).

Y. Huang is with the State Key Laboratory of Power System, Department of Electrical Engineering, Tsinghua University, Beijing 100084, China (e-mail: yulonghuang@mails.tsinghua.edu.cn).

R. Li and Q. Wang are with the XJ Electric Corporation Ltd., Xuchang 461000, China (e-mail: ruishengl@139.com; wangqp@epri.sgcc.com.cn).

Color versions of one or more of the figures in this paper are available online at http://ieeexplore.ieee.org.

Digital Object Identifier 10.1109/TPEL.2018.2797243

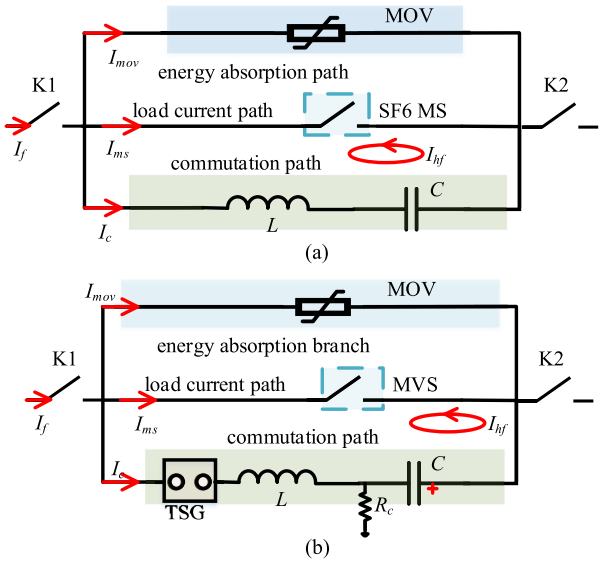

Fig. 1. Topology of mechanical DCCB based on different current commutation methods: (a) Mechanical DCCB with the self-excited oscillation. (b) Mechanical DCCB with the active-excited oscillation.

6 kA. Besides, the regular SF6 MS has features of long stroke and heavy-moving parts [15], resulting in the operating time of this kind of mechanical DCCB is in the order of tens of milliseconds. Therefore, in aspects of the current interruption ability and the operating time, mechanical DCCBs based on self-excited oscillation cannot satisfy the requirements of the VSC-MTDC system, and they are usually used as transfer breakers in point to point dc system based on the line commutated converters, such as metallic return transfer breakers, ground return transfer breakers, neutral bus switches, and neutral bus ground switches [8], [9].

Aimed to increase the current interruption ability and shorten the operating time, an active-excited oscillation method is proposed to realize the current commutation in mechanical DCCBs shown in Fig. 1(b), [10]–[12]. In Fig. 1(b), MVS is a mechanical vacuum switch in the load current path; TSG is a triggering sphere gap; C is a precharged capacitor; L is a reactor; $I_{\rm hf}$ is the active excited oscillatory current in the closed circuit with the load current path and the commutation path in series. As shown in Fig. 1(b), by igniting TSG, $I_{\rm hf}$ is produced by the discharge of C through L, TSG, and MVS. With merits of excellent arc extinguishing characteristics, small stroke, and light-moving parts [14]–[16], vacuum interrupter instead of SF6 interrupter is employed to make sure that the fault current can be reliably commutated at zero-crossing points and the operating time of mechanical DCCBs is less than 5 ms. The current commutation and interruption ability of mechanical DCCBs is defined as the peak value of $I_{\rm hf}$, and with other parameters determined, it can be enlarged by increasing the precharged voltage on C. By using the active-excited oscillation method to increase the current interruption ability and by using MVS instead of the regular SF6 MS to shorten the operating time, the mechanical DCCB shown in Fig. 1(b) is satisfactory for MTDC grids, but when it is used in practical engineering, following problems show up.

As mentioned, C in Fig. 1(b) should be charged to a preset voltage. The maximum voltage on C equal to the clamping voltage of MOVs (1.5 p.u., in the order of several hundreds of kV) is so high that online charging system is used. In Fig. 1(b), with K1, MVS closed and K2 open, C is charged by dc bus through the charging resistor $R_{\rm c}$. After C is charged to the preset voltage (system rating voltage), K2 is closed to conduct the load current. In situations when the voltage of dc bus is unstable, especially lower than the system rating voltage, the precharged voltage on C is not equal to the preset voltage, resulting in working uncertainties of the mechanical DCCB. In [12], to obtain the bidirectional dc interruption ability, TSG with weak arc extinguishing capability is used. With TSG arcing in air, fire accidents are possible. In addition, with the arc extinguishing capability of TSG uncertain, the voltage on C after current interruption is invariable, resulting in the instability of its autoreclosing function. More notably, as the arc extinguishing capacity of TSG is too weak, a residual current through the commutation path will oscillate continuously until it is interrupted by K1 and K2, and long-time burning of TSG is inevitable, resulting in a short lifetime.

Focused on the current commutation problem in the mechanical DCCB, to overcome shortcomings of the existing current commutation methods, this paper has investigated a novel mechanical DCCB. The rest of this paper is organized as follows. The structure and working principle of the novel mechanical DCCB are first presented in Section II-A, simulation model of the novel mechanical DCCB established in PSCAD is introduced in Section III. Based on the theoretical analysis of simulation results, detailed transient characteristics of current interruption process of the novel mechanical DCCB are revealed. In Section IV, to verify the theoretical analysis and the feasibility of the novel mechanical DCCB, current interruption tests have been carried out on the prototype that was developed in our lab. Then, in Section V, failures that occurred in the initial experiments have been discussed and protection measures to avoid these failures are proposed. In the end, Section VI concludes this paper.

II. Novel Mechanical DCCB

A. Structure of Novel Mechanical DCCB

Topology of the novel mechanical DCCB is shown in Fig. 2, and it also consists of three paths. Compared with the mechanical DCCB shown in Fig. 1(b), the load current path and the energy absorption path have not changed, but the commutation path is different.

In Fig. 2, C in the commutation path is not precharged. Reactor in the commutation path shown in Fig. 1(b) has been removed. l_0 in Fig. 2(a) is the stray inductance of the commutation path. Instead of TSG in Fig. 1(b), a current commutation drive circuit (CCDC) proposed by us is used in Fig. 2(a). According to the detailed diagram of CCDC illustrated in Fig. 2(b), CCDC consists of a precharged capacitor C_1, a fast-closing switch (FCS), and an air-core transformer (ACT). In Fig. 2(b), L_1 is the primary coil of ACT, r_1 is the stray resistor of the primary side circuit, L_2 is the secondary coil of

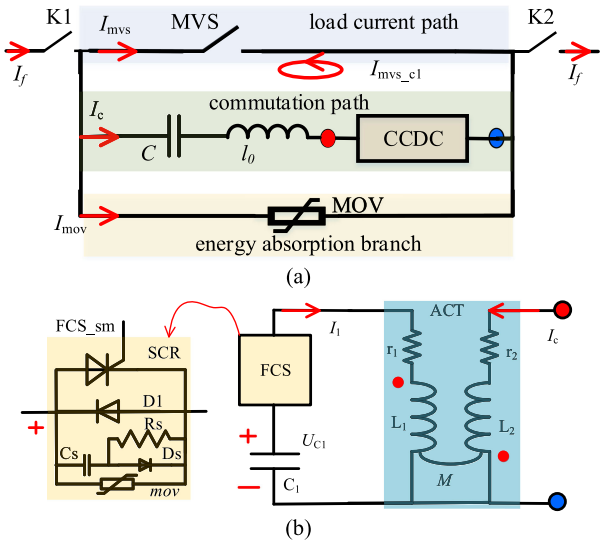

Fig. 2. Structure of novel mechanical DCCB; (a) the overall topology of novel mechanical DCCB; (b) detailed diagram of CCDC. The red circle is the in-port of CCDC, and the blue circle is the out-port of CCDC.

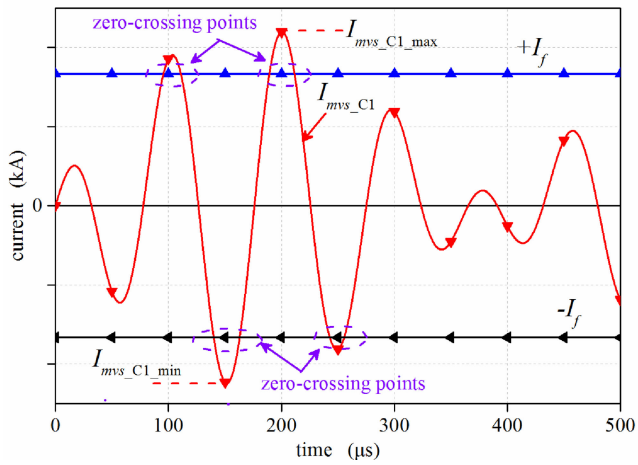

Fig. 3. Typical current waveforms during the current commutation process.

ACT, r_2 is the stray resistor of the secondary side circuit, M is the mutual inductance between L_1 and L_2. C_1 is in series with L_1 through FCS. L_2 is in series with C in the commutation path.

The maximum voltage on C_1 equal to the precharged voltage U_{C10} is usually lower than 10 kV, so charging system for C_1 can be designed independently. Compared with the online charging system for precharged C in Fig. 1(b), the independent charging system for C_1 is simpler and cheaper. Besides, the independent charging system can make sure that U_{C10} is stable and the working state of the mechanical DCCB is certain and predictable. As shown in Fig. 2(b), FCS consists of several submodules (FCS_sm) in series. The FCS_sm, capable of conducting bidirectional currents, is composed of four paralleled branches, including a thyristor (SCR), an antiparalleled diode (D1), an RCD snubber circuit and an mov. RCD snubber circuit is used to mitigate the transient recovery voltage on FCS_sm during its turn-OFF process, and suppress the surge current through SCR produced by the discharge of C_s during its turn-on process. Different from TSG used in Fig. 1(b), FCS is controllable, and without arcing in the air, FCS is safer for practical application in power system than TSG. Thus, without using TSG and the online charging system for C, the reliability of the novel mechanical DCCB with CCDC is improved. Considering that the cost of the mechanical DCCB is mainly decided by the energy capacity of C, by using CCDC for current commutation, parameters of C has not been changed and the cost of the mechanical DCCB will change a little.

B. Current Commutation Principle of Novel Mechanical DCCB

Compared with the existing mechanical DCCB shown in Fig. 1(b), the operation time sequence is unchanged and only the current commutation principle of the novel mechanical DCCB with CCDC is quite different. The current commutation principle is described as follows: Once a fault is detected, contacts of MVS are first commanded to separate. Then with MVS arcing and FCS turned ON, a continuous oscillatory current I_1 is produced by the discharge of C_1 through FCS and L_1, and meanwhile, an oscillatory current $I_{\mathrm{mvs\_C1}}$ is excited in the closed circuit with MVS, C, l_0, r_2, and L_2 in series, as shown in Fig. 2(a). The typical waveform of I_{mvs_C1} is illustrated in Fig. 3. $+I_{\mathrm{f}}$ is the positive fault current through the mechanical DCCB, which flows from left to right, just as shown in Fig. 2(a). $-I_{\mathrm{f}}$ is the negative fault current through the mechanical DCCB, which flows from right to left. Before the current commutation, the fault current is completely conducted by MVS, and I_{f} is equal to I_{mvs}.

As shown in Fig. 3, FCS is turned ON at 0 μs. During the current commutation process, I_{mvs_C1} is continuously oscillating and I_f is almost constant. The total current through MVS I_{mvs} during this period is the superposition of I_f and I_{mvs_C1}. As long as I_f is larger than the minimum value of I_{mvs_C1} ($\mathrm{I}_{mvs\_C1\_\mathrm{min}}$) and smaller than the maximum value of I_{mvs_C1} ($\mathrm{I}_{mvs\_C1\_\mathrm{max}}$), I_{mvs} will pass through zero. With I_{mvs} extinguished by the arcing MVS at the current zero-crossing point, the current can be completely commutated from the load current path to the commutation path. The detailed transient current interruption process of the novel mechanical DCCB will be revealed based on simulation and experimental results in the following sections.

III. Simulation of the Novel Mechanical DCCB

In VSC-MTDC systems, during the initial period of short-circuit fault, the surge current is mainly produced by the discharge of the capacitors in converter [1], [3]–[4]. When a short-circuit fault occurs at the outlet of DCCB, the peak value and the rise rate of the fault current are the largest, and the working condition of DCCB in this case is most severe. The equivalent circuit of the extreme case is illustrated in Fig. 4.

As shown in Fig. 4, one DCCB is installed at the positive pole, and the other is installed at the negative pole [1]. C_{DC} is the equivalent capacitance of the converter. For the extreme case, the inductance of the short transmission line is negligible, and

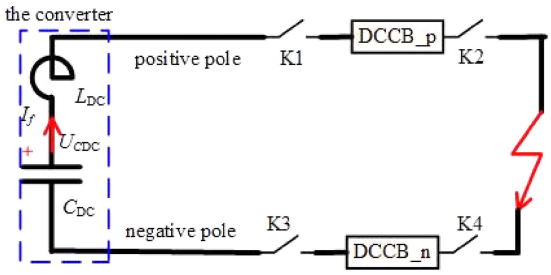

Fig. 4. Equivalent circuit of the extreme case.

TABLE I
PARAMETERS OF NOVEL MECHANICAL DCCB PROTOTYPE WITH CCDC

Items	Values	Items	Values
C_1 (μF)	58	C (μF)	24
l_1 (μH)	2.5	l_0 (μH)	5
L_1 (μH)	1.96	L_2 (μH)	2.33
r_1 (m)Ω	20	r_2 (m)Ω	40
U_{C10} (kV)	4	M (μH)	1.95

the current limiter made of reactors is not installed at the outlet of the converter. Therefore, L_{DC} is the equivalent inductance of the six bridge reactors in the converter. According to electrical parameters of the demonstration MTDC projects, such as Nan'ao and Zhoushan projects in China [1], [19], C_{DC} is in the order of 100 μF and L_{DC} is in the order of 100 mH. The initial voltage on C_{DC} (U_{CDC0}) is the system rating voltage (320 kV for Nan'ao project and 400 kV for Zhoushan project). With C_{DC}, L_{DC}, and U_{CDC0} equal to 100 μF, 100 mH, and 320 kV, a simulation model for the equivalent circuit corresponding to the Nan'ao project is established in PSCAD. Parameters of the novel mechanical DCCB with CCDC in the simulation model are listed in Table I. The simulation results are shown in Fig. 5.

The fault current is ignited by closing the disconnectors (K1, K2, K3, and K4 shown in Fig. 4) at 0 ms, and it is initially conducted by the load current path I_{mvs}. As the contacts of MVS are commanded to separate at 0.1 ms and FCS is turned ON at 2 ms, the fault current is completely commutated to the commutation path I_{c} by CCDC at 2.05 ms. During the period, the current through the commutation path charging C continuously U_{CB} and its rise rate dU_{CB}/dt can be calculated by (1) and (2). The fault current rate dI_f/dt can be calculated by (3)

$$U_{CB} = \int \frac{I_c}{C} dt + U_{L2} \approx \frac{I_c}{C} \Delta t + U_{L2} \tag{1}$$

$$\frac{dU_{CB}}{dt} \approx \frac{I_c}{C} \approx 270\,\mathrm{V}/\mu\mathrm{s} \tag{2}$$

$$\frac{dI_f}{dt} = \frac{1}{L_{\mathrm{DC}}} \left(2 \cdot U_{\mathrm{CB}} - U_{\mathrm{CDC}}\right). \tag{3}$$

As shown in Fig. 5, based on (3), when $2{\cdot}U_{\mathrm{CB}}$ is larger than U_{CDC}, the fault current reaches its peak value and starts to decrease at 2.49 ms. Decided by the intrinsic V–I characteristic of MOV [20], when U_{CB} reaches the knee-point voltage of MOVs at 3.11 ms, the equivalent impedance of MOVs decreases dramatically, resulting in that most of the fault current is

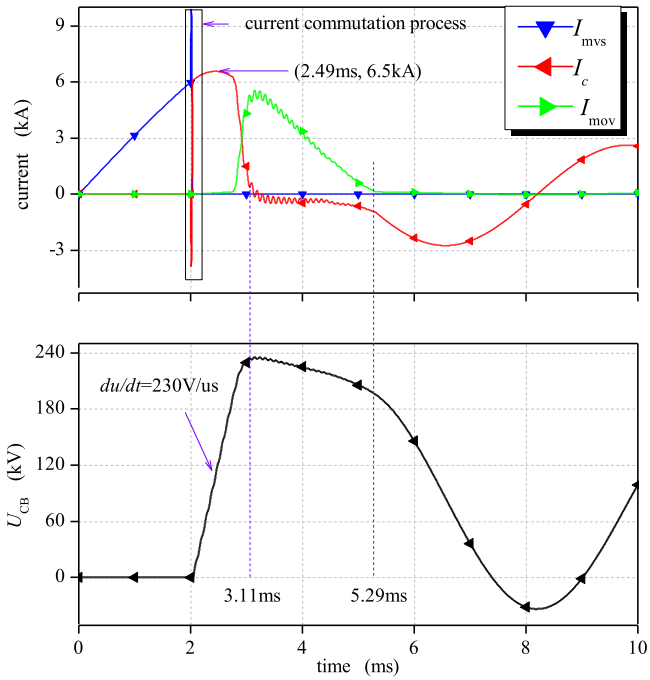

Fig. 5. Simulation results of novel mechanical DCCB in the extreme case.

naturally commutated to the energy absorption path, and U_{CB} is limited to be the clamping voltage of MOVs.

During the period from 3.11 to 5.29 ms, in reference to the V–I characteristic curve of MOVs, with I_{mov} decreasing, U_{CB} equal to the voltage on MOVs decreases slightly. The slight change of U_{CB} results in the transient current oscillation in the closed circuit with the commutation path and the energy absorption path in series. According to (3), with U_{CDC} constant and U_{CB} decreasing slightly, I_{mov} (almost equal to I_f) decreases with a nearly constant rate, just as shown in Fig. 5. During this period, the residual energy stored by L_{DC} is dissipated by MOVs.

At 5.29 ms when U_{CB} decreases to the knee-point voltage of MOVs, the equivalent impedance of MOVs increases rapidly and I_{mov} decreases to almost zero. At this time, with the load current path and the energy absorption regarded as open branches, the novel mechanical DCCB is equivalent to the commutation path which is made of C in series with l_0 and L_2. An oscillation through the circuit with C_{DC}, L_{DC}, C, l_0 and L_2 in series is produced, resulting in the residual continuously oscillatory current and voltage, just as shown in Fig. 5. The oscillatory current can be easily interrupted at zero-crossing points by the disconnectors (K1, K2, K3, and K4) after they are open.

IV. EXPERIMENTS OF THE NOVEL MECHANICAL DCCB

In the simulation model presented in Section III, it is assumed that the dielectric recovery strength of MVS is larger than the transient recovery voltage on MVS (U_{CB}) and no restrikes of MVS occur during the current interruption process. In this part, to verify this assumption and the feasibility of the novel mechanical DCCB, a prototype based on the topology shown in Fig. 2 is established, and its rating voltage is 20 kV. The

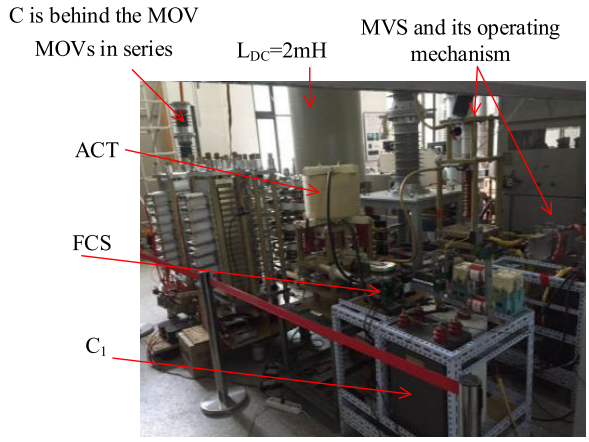

Fig. 6. Pictures of experimental setups and the prototype.

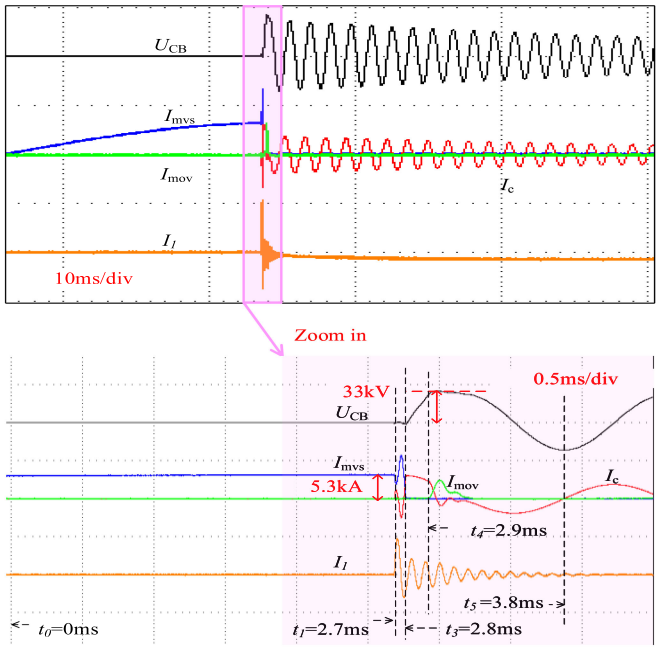

Fig. 7. Current interruption results of DCCB with CCDC.

detailed technology of MVS used in the prototype is introduced in [16].

In reference to the typical experimental circuit for DCCB [21], which is similar to the circuit in Fig. 4, the bidirectional current interruption experiments have been carried out on the prototype. With $C_{\rm DC}$ and $L_{\rm DC}$ equal to 80 mF and 2 mH, a current with frequency of ∼12 Hz is produced to simulate the fault current to be interrupted. The pictures of the experimental setup and the prototype are shown in Fig. 6.

In the tests, when the current reaches ±5.3 kA, the contacts of MVS are commanded to separate at t_0 (0 ms), and FCS is triggered by the regular drive circuit for thyristor at t_1 (2.7 ms). As mentioned, bidirectional currents interruption tests have been carried out. Considering the transient processes of positive current and negative current interruption are similar, only the positive current interruption tests results are demonstrated in Fig. 7.

During the current commutation period, $I_{\rm mvs}$ is the superposition of I_f (5.3 kA) and $I_{\rm mvs\_C1}$, and $I_{\rm c}$ is equal to I_{mvs_C1}. As shown in Figs. 2 and 7, the initial directions of $I_{\rm mvs}$ and $I_{\rm mvs\_C1}$ are opposite, and $I_{\rm mvs}$ decreases immediately after the turn-ON of FCS at 2.7 ms. When $I_{\rm mvs\_C1}$ is equal to I_f, $I_{\rm mvs}$ passes through zero at t_3 (2.75 ms) and it is extinguished by MVS, resulting in the current to be completely commutated to the commutation path. During the short period from t_3 to t_4 ∼ (100 μs), $U_{\rm CB}$ increases continuously with a rise rate of 230 V/μs [≈5.3 kA/24 μF in (2)]. Caused by the charging of C, $U_{\rm CB}$ increases to the knee-point voltage of MOV at t_4 (2.9 ms), resulting in the current to be naturally commutated to the energy absorption path, and $U_{\rm CB}$ is limited to be the voltage on MOVs (∼33 kV). As the energy stored by $L_{\rm CD}$ is absorbed by MOVs and the current decreases gradually, $U_{\rm CB}$ decreases to the knee-point voltage of MOV, resulting in the current to be commutated back to the commutation path. Finally, the oscillation through the closed-circuit with $C_{\rm CD}$, $L_{\rm CD}$, and commutation path in series happens, resulting in the oscillatory current I_c and voltage $U_{\rm CB}$.

The varying patterns of the current waveforms and the voltage waveforms obtained by tests and simulation are consistent. The simulation model therefore has been verified by the experiments. Based on simulation and experimental results, the transient varying patterns of electric parameters, such as the current, the voltage, and the energy, in the mechanical DCCB with CCDC are revealed. Both simulation and experimental results have proved the feasibility of the novel mechanical DCCB with CCDC.

In the experiments, the prototype with rating voltage of 20 kV has interrupted currents of 5.3 kA within 3 ms. To promote the industrial application of the novel mechanical DCCB in the MTDC system, the rating voltage and interruption current of the mechanical DCCB should be improved by increasing the rating voltage of the components and optimizing its parameters. Further research focused on these problems will be carried out in the future.

V. Typical Failures of FCS

In Section IV, tests result with the current successfully interrupted by the novel mechanical DCCB prototype is presented. In fact, in initial experiments, two kinds of failure have occurred. To ensure the reliability of the novel mechanical DCCB and reveal the failure mechanisms, the mathematical model of CCDC during the current commutation process is first introduced and then, the test results are discussed. Finally, relative protection measures to avoid these failures are proposed in this section.

A. Mathematical Model of CCDC

To reveal the failure mechanisms of FCS and obtain the current commutation and interruption ability of the mechanical DCCB with CCDC, it is necessary to establish a mathematical model of CCDC in the mechanical DCCB. Before MVS is extinguished, both the load current path and the branch with $L_{\rm DC}$ and $C_{\rm DC}$ in series are parallel with the commutation path. Considering that for the working frequency of CCDC (several

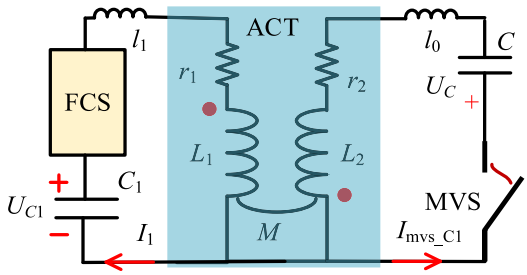

Fig. 8. Equivalent circuit of CCDC during the current commutation process.

kHz), the impedance of the branch with L_{DC} and C_{DC} in series is much larger than that of the load current path which is composed of MVS, the branch with L_{DC} and C_{DC} in series can be regarded as open circuit, and the equivalent circuit of CCDC during the current commutation process is shown in Fig. 8. The state equation of the circuit shown in Fig. 8 is listed in (4).

In (4), U_{FCS} is the voltage drop of the FCS; U_{mvs} is the arc voltage of the MVS; U_C and U_{C1} is the voltage on C and C_1, respectively. l_1 is the stray inductance of the primary side of ACT; l_0 is the stray inductance of the secondary side of ACT. U_{FCS} can be obtained in the datasheet of the used SCR and D; U_{mvs} is usually in the range of 10–25 V [15], which can be measured by experiments. l_1 and l_0 are decided by the physical arrangement of the mechanical DCCB with CCDC

$$\begin{pmatrix} L_1+l_1 & -M & 0 & 0 \\ M & -(L_2+l_0) & 0 & 0 \\ 0 & 0 & 1 & 0 \\ 0 & 0 & 0 & 1 \end{pmatrix} \begin{pmatrix} \frac{dI_1}{dt} \\ \frac{dI_{mvs\_C1}}{dt} \\ \frac{dU_{C1}}{dt} \\ \frac{dU_C}{dt} \end{pmatrix} = \begin{pmatrix} U_{C1}-I_1\cdot r_1-u_{FCS} \\ I_{mvs\_C1}\cdot r_0+u_{mvs}+U_C \\ -\frac{I_1}{C_1} \\ \frac{I_{mvs\_C1}}{C} \end{pmatrix}. \quad (4)$$

B. Discussion of FCS Failures

As mentioned, FCS shown in Fig. 2(b) is made of several FCS_sm in series and each FCS_sm consists of four paralleled branches, including a thyristor (SCR), an antiparalleled diode (D1), an RCD snubber circuit and an mov. SCR can be either electrically triggered or light triggered [22]. In initial experiments, failures occurred in FCS twice. At the first time, D1 was damaged, and at the second time, light triggered SCR was damaged. After the failures, the press pack housing D1 and light triggered SCR were disassembled, and the internal pictures have been shown in Fig. 9(a) and (b). Fortunately, when the failure occurred in D1 and SCR, testing waveforms were captured by oscilloscope DL750, respectively, and they are shown in Fig. 9(c) and (d).

As shown in Fig. 9(a), the failure spot of D1 was near the insulation edge, meaning D1 was probably damaged by the voltage breakdown. According to the test waveforms shown in Fig. 9(c), after the triggering signal for SCR (T_{SCR}) was

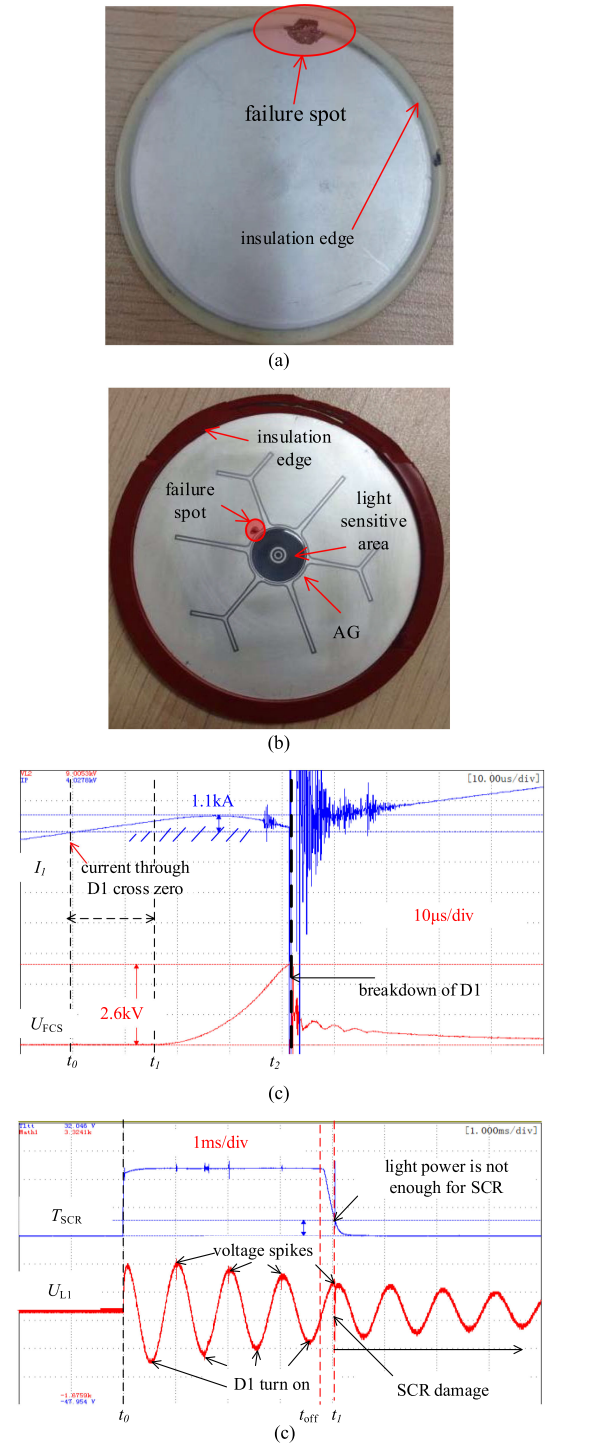

Fig. 9. Testing results of the damaged FCS: (a) Picture of the damaged D1, (b) picture of the damaged light triggering SCR, (c) current and voltage waveforms when D1 is damaged, and (d) current and voltage waveforms when SCR was damaged.

withdrawn and SCR was turned OFF, the current through D1 passed across zero at t_0. D1 with regular recovery speed could not recover its dielectric strength immediately during the period from t_0 to t_1, so a reverse current was conducted by D1 and the voltage on D1 (U_{FCS}) was almost zero. With the charge carriers in D1 being pulled out, the reverse dielectric strength

of D1 increased gradually and the current was commutated to RCD snubber circuit. In the closed circuit with C_1, C_s, D_s, and L_1 in series, caused by the current charging C_s, $U_{\rm FCS}$ started to increase at t_1 with a rise rate of 100 V/ μs. $U_{\rm FCS}$ competed with the reverse dielectric strength of D1, and at t_2 when $U_{\rm FCS}$ reaches 2.6 kV, $U_{\rm FCS}$ exceeded the dielectric strength of D1, resulting in the voltage breakdown of D1.

Based on the tests results, the failure mechanism of D1 is that the dielectric recovery speed of D1 is slower than the rise rate of $U_{\rm FCS}$. Two solutions to avoid the failure of D1 are proposed as follows: 1) with the rise rate of $U_{\rm FCS}$ unchanged, the fast recovery diode can be used to obtain higher dielectric recovery speed; 2) considering that $U_{\rm FCS}$ is produced by the redistribution of the residual energy on C_1, if $T_{\rm SCR}$ is not withdrawn until the residual energy stored by C_1 is nearly completely consumed through the damping circuit, the final value of $U_{\rm FCS}$ will be almost zero and the breakdown of D1 can be avoided.

By adopting the proposed measures, the damage of D1 has been avoided, but the failure of the light triggered SCR happened, just as shown in Fig. 9(b). The failure spot of SCR was near the amplifying gates, which implied that SCR might be damaged by high *di/dt* [22].

The damage process of SCR caused by high *di/dt* is described as follows: During the turn-ON process of SCR, the current is first concentrated in the small region near AGs and then it spreads to the whole wafer quickly. When turning on a current with over large rise rate (*di/dt*), the spread speed of the current is not high enough, resulting in current filamentation. Thermal losses of this current concentration spot are so high that the thermal damage of SCR is inevitable.

However, by solving the state equation shown in (4), we found that during the tests, the rise rate of the current through SCR (I_1) was in the order of 100 A/μs, which was much lower than the *di/dt* capability of SCR. To find out the failure mechanism of SCR, tests waveforms illustrated in Fig. 9(d) are analyzed. $T_{\rm SCR}$ is the light triggering signal for SCR and U_{L1} is the voltage on L_1.

By analyzing the equivalent circuit of CCDC shown in Fig. 8, when U_{L1} reaches its positive peaks, I_1 passes across zero from negative to positive, and at this time, SCR is turned ON with the current commutated from D1 to SCR. When U_{L1} reaches its negative peaks, I_1 passes across zero from positive to negative, and at this time, D1 is turned ON with the current commutated from SCR to D1. As presented in Fig. 9(d), during the period from t_0 to t_1, the current commutation from D1 to SCR which was characterized by the voltage spikes showing up when U_{L1} reached its positive peaks. In the experiments, a command to withdraw $T_{\rm SCR}$ was sent out at $t_{\rm off}$ and $T_{\rm SCR}$ started to decease. But it did not drop to zero at t_1. A forward blocking voltage was applied to SCR at t_1 when $T_{\rm SCR}$ was very small. Considering that the current spread speed at the initial turn-ON process of SCR is proportional to the light power of $T_{\rm SCR}$, SCR was turned ON at t_1 with a lower current spread speed, resulting in the formation of current filamentation and SCR was burned by the heat produced at the current concentration spot. After t_1, the damaged SCR could conduct the oscillatory current and the current commutation from D1 to SCR did not happen which could be verified by the disappearance of voltage spikes.

In conclusion, the reason for the failure of SCR is that light triggered SCR is forced to turn ON when the light power of $T_{\rm SCR}$ is lower than the standard value. Therefore, $T_{\rm SCR}$ should be designed to decrease to zero abruptly so that it can be avoided that SCR is turned on with lower light triggering power.

After adopting the proposed measures, failures of D1 and SCR in FCS have been avoided. With FCS working normally, current interruption tests have been successfully carried out on the novel mechanical DCCB prototype shown in Section IV. It is worth mentioning that full-controlled semiconductors, such as gate turn-off thyristor, insulated gate bipolar transistor, injection-enhanced gate transistor, and integrated gate-commutated thyristors, have higher *di/dt* capacity and dielectric recovery speed after their turn-OFF. By replacing SCR and D1 with the full-controlled semiconductor, the failures can also be easily avoided and the reliability of FCS can be improved. However, the full-controlled semiconductor is much more expensive than regular SCR and fast diode, so in the experiments, the measures mentioned before were used to avoid the failures.

VI. Conclusion

Focused on the current commutation difficulty from the load current path to the commutation path, a novel mechanical DCCB with CCDC is investigated in this paper. In comparison with traditional mechanical DCCBs, the charging system and the current commutation method for the novel mechanical DCCB are simpler and more reliable. The structure and working principle of the novel mechanical DCCB with CCDC are introduced first. Then, a simulation model of the novel mechanical DCCB was established in PSCAD and by analyzing the simulation results, the detailed transient varying patterns of the electric parameters, such as the current, the voltage, and the energy in the novel mechanical DCCB during its current interruption process have been revealed. To verify the simulation model and the feasibility of the novel mechanical DCCB, a prototype was developed and relative current interruption tests have been carried out on the prototype. According to tests results, the novel mechanical DCCB prototype can interrupt a current of 5.3 kA within 3 ms. In the end, the failures that occurred in the novel mechanical DCCB in the initial experiments are discussed, and by revealing the failures mechanism, protection measures to avoid these failures have been proposed to ensure the reliability of the mechanical DCCB.

References

[1] J. Liu *et al.*, "A hybrid current-limiting circuit for DC line fault in multiterminal VSC-HVDC system," *IEEE Trans Ind. Electron.*, vol. 64, no. 7, pp. 5595–5607, Jul. 2017.

[2] C. M. Franck, "HVDC circuit breakers: A review identifying future research needs," *IEEE Trans. Power Del.*, vol. 26, no. 2, pp. 998–1007, Apr. 2011.

[3] Z. Zhang and Z. Xua, "Short-circuit current calculation and performance requirement of HVDC breakers for MMC-MTDC systems," *IEEJ Trans. Elect. Electron. Eng.*, vol. 11, no. 2, pp. 168–177, 2016.

[4] O. Cwikowski *et al.*, "Fault current testing envelopes for VSC HVDC circuit breakers," *IET Gener., Transmiss., Distrib.*, vol. 10, no. 6, pp. 1393–1400, 2016.
[5] H. Melios and T. Vladimir, "Transient fault studies in a multi-terminal VSC-HVDC grid utilizing protection means through DC circuit breakers," in *Proc. Int. Conf. Grenoble PowerTech*, Grenoble, France, Jun. 2013, pp. 1–6.
[6] J. Häfner and B. Jacobson, "Proactive hybrid HVDC breakers—A key innovation for reliable HVDC grids," in *Proc. Int. Conf. CIGRÉ Symp.*, Bologna, Italy, Sep. 2011 pp. 264–273.
[7] A. N. Greenwood, P. Barkan, and W. C. Kracht, "HYDC vacuum circuit breakers," *IEEE Trans. Power App. Syst.*, vol. PAS-91, no. 4, pp. 1575–1588, Jul. 1972.
[8] H. Nakao *et al.*, "D.C. current interruption in HVDC SF6 Gas MRTB by means of self-excited oscillation superimposition," *IEEE Trans. Power Del.*, vol. 16, no. 4, pp. 687–693, Oct. 2001.
[9] K. Zhu, X. Li, S. Jia, W. Zhang, and W. Gao, "Study of the switching arc characteristics of a 500 kV HVDC self-excited oscillatory metallic return transfer breaker," *IEEE Trans. Dielectrics Electr. Insulation*, vol. 22, no. 1, pp. 128–134, Feb. 2015.
[10] Z. Q. Shi *et al.*, "Investigation on DC interruption based on artificial current zero of vacuum switch," in *Proc. 24th Int. Symp. Discharges Elect. Insul. Vacuum*, 2010, pp. 158–161.
[11] Y. K. Zhang, Z. Q. Shi, S. L. Jia, X. C. Song, and L. J. Wang, "Simulation and analysis on the interruption process of HVDC vacuum switch with forced current zero," in *Proc. 26th Int. Symp. Discharges Elect. Insul. Vacuum*, Mumbai, India, 2014, pp. 281–284.
[12] Z. Q. Shi, Y. K. Zhang, S. L. Jia, X. C. Song, L. J. Wang, and M. Chen, "Design and numerical investigation of A HVDC vacuum switch based on artificial current zero," *IEEE Trans. Dielect. Elect. Insul.*, vol. 22, no. 1, pp. 135–141, Feb. 2015.
[13] S. Yanabu, T. Tamagawa, S. Irokawa, T. Horiuchi, and S. Tomimuro, "Development of HVDC circuit breaker and its interrupting test," *IEEE Trans. Power App. Syst.*, vol. PAS-101, no. 7, pp. 1958–1965, Jul. 1982.
[14] T. Senda, T. Tamagawa, K. Higuchi, T. Horiuchi, and S. Yanabu, "Development of HVDC circuit breaker based on hybrid interruption scheme," *IEEE Trans. Power App. Syst.*, vol. PAS-103, no. 3, pp. 545–552, Mar. 1984.
[15] W. Wen *et al.*, "Research on current commutation measures for hybrid DC circuit breakers," *IEEE Trans. Power Del.*, vol. 31, no. 4, pp. 1456–1463, Aug. 2016.
[16] W. Wen *et al.*, "Research on operating mechanism for ultra-fast 40.5 kV vacuum switches," *IEEE Trans. Power Del.*, vol. 30, no. 6, pp. 2553–2560, Dec. 2015.
[17] J. M. Anderson and J. J. Carroll, "Applicability of a vacuum interrupter as the basic switch element in HVDC breakers," *IEEE Trans. Power App. Syst.*, vol. PAS-97, no. 5, pp. 1893–1900, Sep. 1978.
[18] L. Luhui *et al.*, "The characteristics of vacuum arc in the process of DC interruption using butt contacts and TMF contacts," *IEEE Trans. Plasma Sci.*, vol. 42, no. 6, pp. 1736–1741, Jun. 2014.
[19] H. Rao, "Architecture of Nan'ao multi-terminal VSC-HVDC system and its multi-functional control," *CSEE J. Power Energy Syst.*, vol. 1, no. 1, pp. 9–18, 2015.
[20] V. S. Brito, G. R. S. Lira, E. G. Costa, and M. J. A. Maia, "A wide-range model for metal-oxide surge arrester," *IEEE Trans. Power Del.*, vol. 33, no. 1, pp. 102–109, Feb. 2018.
[21] A. Hassanpoor, J. Hafner, and B. Jacobson, "Technical assessment of load commutation switch in hybrid HVDC breaker," *IEEE Trans. Power Electron.*, vol. 30, no. 10, pp. 5393–5400, Oct. 2015.
[22] J. Vobecký *et al.*, "Silicon thyristors for ultrahigh power (GW) applications," *IEEE Trans. Electron Devices*, vol. 64, no. 3, pp. 760–768, Mar. 2017.

Weijie Wen was born in Shandong, China, in 1989. She received the B.S. degree in electrical engineering from Sichuan University, Chengdu, China, in 2012, and the Ph.D. degree in electrical engineering from Tsinghua University, Beijing, China, in 2017.

She is currently a Lecturer with the Key Laboratory of Smart Grid of Ministry of Education, Tianjin University, Tianjin, China. She is currently working in the fields of fast mechanical switches, current limiters, and direct current circuit breakers.

Yizhen Wang received the B.E.E. degree in electrical engineering from Tianjin University, Tianjin, China, in 2010, the M.E.E. degree in electrical engineering from the China Electric Power Research Institute, Beijing, China, in 2013, and the Ph.D. degree in electrical engineering from Tsinghua University, Beijing, in 2017.

He is currently a Lecturer in Electrical Engineering with Tianjin University. His research interests include power system stability analysis, high-power electronics, and VSC-HVDC systems.

Bin Li received the B.Sc., M.Sc., and Ph.D. degrees in electrical engineering from Tianjin University, Tianjin, China, in 1999, 2002, and 2005, respectively.

He is currently a Professor with the School of Electrical Engineering and Automation, Tianjin University. His main research field is involved in the protection and control of power systems and microgrids.

Yulong Huang was born in Hubei, China, in 1964. He received the B.S. degree in electrical engineering from Hunan University, Changsha, China, in 1985, and the M.Sc. degree from the Department of Electrical Engineering, Tsinghua University, Beijing, China, in 1991.

He is currently an Associate Professor with the Department of Electrical Engineering, Tsinghua University.

Ruisheng Li received the M.Eng. degree in power system from Xi'an Jiaotong University, Xi'an, China, in 1984.

He is currently the Deputy Chief Engineer with XJ Electric Corporation Ltd., Xuchang, China, and the Deputy Director of the Smart Grid Research Center, XJ Electric Corporation Ltd. He holds eight patents and has authored and coauthored more than 30 papers. He was responsible for more than 20 national, provincial, and ministerial projects, and drafted 3 national standards and 3 industry standards.

Mr. Li worked in power system for 25 years, and was the recipient of numerous awards, including the Grand Prize of National Scientific and Technological Progress in 2012.

Qingping Wang received the Ph.D. degree in electrical engineering from Tianjin University, Tianjin, China, in 2002.

From 2002 to 2004, he was a Postdoctor with Tsinghua University, Beijing, China. From 2004 to 2005, he was an R&D engineer with ALSTOM T&D, U.K. Since 2005, he has been with State Grid and is currently the Deputy Director General of corporate R&D, XJ Group. During this period, he worked in ABB corporate research and Global Energy Interconnection Development & Corporation Organization for a few years. His current research interests include smart distribution and utilization, hybrid AVC/dc networks, and integrated energy systems.